

Retinal Structure of Birds of Prey Revealed by Ultra-High Resolution Spectral-Domain Optical Coherence Tomography

Marco Ruggeri, James C. Major, Jr, Craig McKeown, Robert W. Knighton, Carmen A. Puliafito, and Shuliang Jiao

PURPOSE. To reveal three-dimensional (3-D) information about the retinal structures of birds of prey in vivo.

METHODS. An ultra-high resolution spectral-domain optical coherence tomography (SD-OCT) system was built for in vivo imaging of retinas of birds of prey. The calibrated imaging depth and axial resolution of the system were 3.1 mm and 2.8 μm (in tissue), respectively. 3-D segmentation was performed for calculation of the retinal nerve fiber layer (RNFL) map.

RESULTS. High-resolution OCT images were obtained of the retinas of four species of birds of prey: two diurnal hawks (*Buteo platypterus* and *Buteo brachyurus*) and two nocturnal owls (*Bubo virginianus* and *Strix varia*). These images showed the detailed retinal anatomy, including the retinal layers and the structure of the deep and shallow foveae. The calculated thickness map showed the RNFL distribution. Traumatic injury to one bird's retina was also successfully imaged.

CONCLUSIONS. Ultra-high resolution SD-OCT provides unprecedented high-quality 2-D and 3-D in vivo visualization of the retinal structures of birds of prey. SD-OCT is a powerful imaging tool for vision research in birds of prey. (*Invest Ophthalmol Vis Sci.* 2010;51:5789-5795) DOI:10.1167/iovs.10-5633

Birds and particularly birds of prey are known for their unique retinal structures. Although the arrangement of retinal layers in birds is the same as in other vertebrates,¹ variations in the morphology of the retina, the regions of highest visual acuity and the retinal vascularization are significant.^{1,2} The visual acuity of birds is improved by the structure of the retina itself, in which the density of functional photoreceptors (number of cones and rods per unit area) can be several times that in humans.³⁻⁶ The relative number of cones per rod is usually higher in diurnal species. Therefore, the retina of diurnal birds is consistently rich in cones and exhibits higher visual acuity. In contrast, the retinas of nocturnal birds have a greater relative density of rod photoreceptors, which implies high visual sensitivity.^{7,8} Many avian species have regions within the retina in which the density of the functional photoreceptors is higher and that contain a predominance of

cones over rods. These areas of the retina are known as foveae, and they are specialized for increased visual acuity.^{1,9,10} Two foveas are present in various diurnal birds, including birds of prey (hawks, eagles, and falcons): a deep fovea (nasal/central region) and a shallow fovea (temporal region).^{1,11-14} The central fovea presents a higher density of photoreceptors and generally a steeper and deeper depression compared with the temporal fovea.^{2,10,11} Findings in studies have suggested a greater visual acuity at the central fovea than at the shallow fovea. Some exceptions to bifoveality occur in species of birds of prey such as owls, which have only one fovea, located in the temporal region. Another unique feature of the foveae of owls is that they present a relatively higher density of rod photoreceptors, which is a distinctive feature of nocturnal avian species. The retinas of birds are anangiotic, and nourishment is mainly supplied from a highly vascularized body known as the pecten oculi, whereas oxygenation is received from the choriocapillaris.⁸ The pecten extends from the optic nerve head (ONH) into the vitreous body of the eye, and this vascular structure is larger and more elaborated in diurnal birds than in nocturnal ones.^{2,8} The avascular structure of the retina provides a low-scattering passage for light to travel from the retinal surface to the photoreceptors and thus ensures the sharpest vision.

Although examinations of the eye of birds of prey have been performed with various methods,¹⁵ information about the anatomic structure of the retina of birds in general is relatively modest compared with that for mammalian retina. Since the retina of birds is considered one of the most specialized of any animal species,^{2,8} in vivo examination of its structure has significant importance for vision research.

Although optical coherence tomography (OCT) has been used to image retinas in animals,¹⁶⁻¹⁹ high-resolution spectral-domain OCT (SD-OCT) imaging has not been reported in avian species. In the present study, we demonstrated the application of high-resolution SD-OCT for noninvasive, noncontact, in vivo retinal imaging of birds of prey.

MATERIAL AND METHODS

Ultra-High Resolution OCT Imaging System

OCT is a low-coherence interferometer-based noninvasive microscopic imaging modality that can provide noncontact, high-resolution, cross-sectional images of biological tissues. Analogous to ultrasound B-mode imaging, which detects the ultrasonic echo reflected from the tissue, OCT detects the back-reflected photons in the tissue and constructs cross-sectional images by scanning the probing light. Since it was first reported two decades ago, OCT has been used in a variety of medical research and diagnostic applications, the most successful being in ophthalmology for retinal cross-sectional imaging. Commercial OCT machines are now one of the new standards for in vivo noninvasive

From the Bascom Palmer Eye Institute, University of Miami Miller School of Medicine, Miami, Florida.

Supported in part by National Eye Institute P30 Core Grant EY014801 and National Institutes of Health Grant 1R21 EB008800-01. Submitted for publication April 1, 2010; revised May 16, 2010; accepted May 28, 2010.

Disclosure: **M. Ruggeri**, None; **J.C. Major, Jr**, None; **C. McKeown**, None; **R.W. Knighton**, None; **C.A. Puliafito**, None; **S. Jiao**, None

Corresponding author: Shuliang Jiao, Department of Ophthalmology, Keck School of Medicine, University of Southern California, 1450 San Pablo, Los Angeles, CA 90033; sjiao@usc.edu.

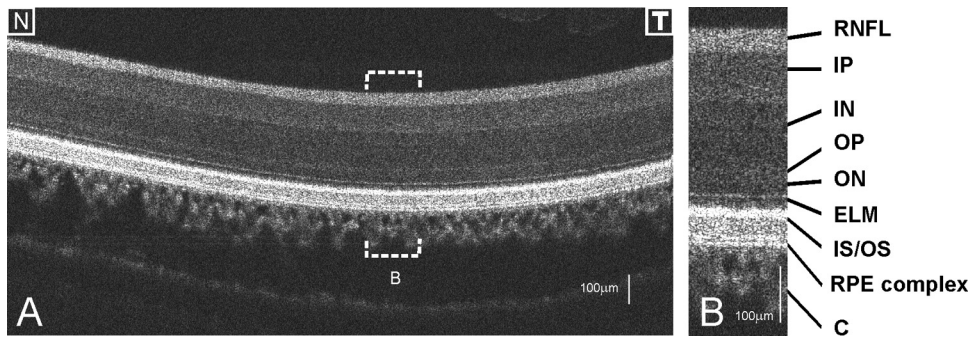


FIGURE 1. (A) OCT image of the left eye of a broad-winged hawk retina. (B) Magnification ($\times 2$) of the bracketed area in (A). The retinal structures are labeled from the *top* to the *bottom* as retinal nerve fiber layer (RNFL), inner plexiform layer (IP), inner nuclear layer (IN), outer plexiform layer (OP), outer nuclear layer (ON), external limiting membrane (ELM), junction between the inner and outer segment layers of the photoreceptors (IS/OS), the RPE complex, and the choroid (C).

ophthalmic imaging and are widely used for diagnosis and treatment monitoring of various ocular diseases in human. There are two detection techniques in OCT: time-domain and spectral domain. Spectral-domain detection is the most recent technology, and it provides much faster imaging speed over time-domain techniques.

The configuration of the OCT system and the image delivery system are similar to those reported before,¹⁶ except that the optical components were modified to accommodate a broader bandwidth. A three-module, superluminescent diode (SLD) light source (Broadlighter, T840-HP; Superlumdiodes Ltd., Moscow Russia) with a center wavelength of 840 nm and an FWHM (full width at half maximum) bandwidth of 100 nm was used. The low-coherence light was coupled into a fiber-based Michelson interferometer that consisted of a 2×2 3 dB fiber coupler that splits the light into the reference arm and the sample arm. The sample light was delivered to a modified optical head of an OCT 2 system (Carl Zeiss Meditec, Inc., Dublin, CA), which consisted of a fundus camera, X-Y galvanometer scanner, and the optics for delivering the sample light into the bird retina and collecting the back-reflected sample light. A double-aspheric 60-D lens (Volk Optical, Inc., Mentor, OH) was used as the objective lens. The power of the sample light was lowered to 750 μ W by adjusting the source power with an attenuator, to ensure that the light intensity delivered to the eye was safe for the retina. The calibrated imaging depth was 3.1 mm. An image acquisition board acquired the image captured by the camera and transferred it to a computer workstation (IntelliStation Z Pro, dual 3.6 GHz processor, 3 GB memory; IBM, Armonk, NY) for signal processing and image display. A complete raster scan consisting of 65,536 scanning steps took approximately 2.7 seconds when the A-line (depth scan) rate of the OCT system was set to be 24 kHz. At this operating condition, the measured sensitivity was approximately 95 dB. The calibrated axial resolution of the system was ~ 3.8 μ m in the air, corresponding to ~ 2.8 μ m in the tissue (the refractive index of the retina is taken to be 1.35). The scan angle was approximately 32° for imaging the retina of raptors. The actual scan length on the retina could not be estimated, because details of size and focal length of the eye of the birds of prey that we imaged are unknown.

Animal Imaging

We performed experiments on two diurnal hawks (the broad-winged hawk *Buteo platypterus* and the short-tailed hawk *Buteo brachyurus*) and two nocturnal owl species (the great horned owl *Bubo virginianus* and the barred owl *Strix varia*). The captive birds were under the care of a handler from MMS (Miami Museum of Science, Falcon Batchelor Bird of Prey Center) with all Federal/USFWS (U.S. Fish and Wildlife Service) permits. All experiments were performed in compliance with the ARVO Statement for the Use of Animals in Ophthalmic and Vision Research, as well as the guidelines of the University of Miami Institutional Animal Care and Use Committee (IACUC) and the Miami Museum of Science. The birds were awake and alert during the entire imaging process. They were held gently by the experienced bird handler, and no mechanical device was used to fix the head. Good animal handling skills provided by MMS prevented the raptors from being harmed and kept them steady during imaging. The imaging room was kept dark to make the birds comfortable and enlarge the pupil. Imaging was guided through the fundus camera and the real-time OCT display. Raster scan patterns consisting of 2048×32 (horizontal \times vertical) and 512×128 depth scans (A-lines) were performed. No multiple scan averaging of the OCT images was used. In addition to the cross-sectional images, an en face fundus image was generated from the OCT data set.²⁰

RESULTS AND DISCUSSION

We first describe images of the retina of a broad-winged hawk. Figure 1A shows one of the cross-sectional images from the acquired 3-D dataset for the left eye of the hawk. The image consists of 2048 A-lines and is displayed in grayscale. Figure 1B shows an enlarged view of the area marked in Figure 1A. Most of the anatomic layers of the hawk retina can be clearly recognized in the OCT image. Layers consisting of nerve fibers or plexiform layers are optically backscattering, whereas nuclear layers are weakly backscattering. We labeled the retinal layers

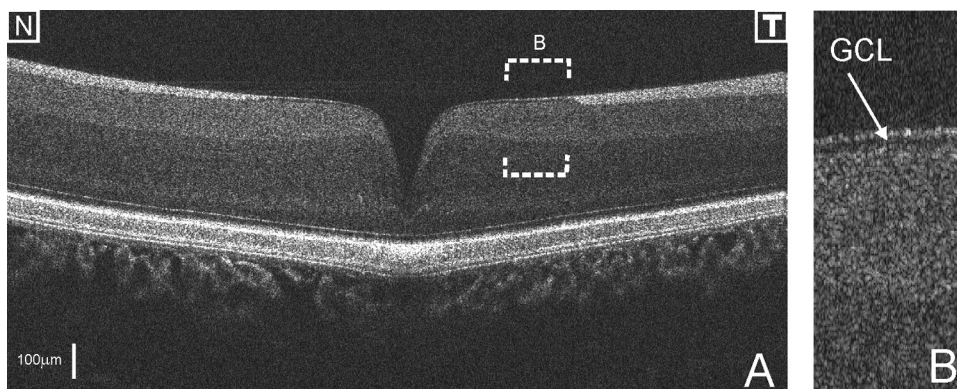


FIGURE 2. (A) OCT image of the retina crossing the deep fovea of the left eye of a broad-winged hawk. The image consists of 2048 A-lines. (B) Enlarged view of the area marked in (A) and the GCL (arrow). Magnification, $\times 4$.

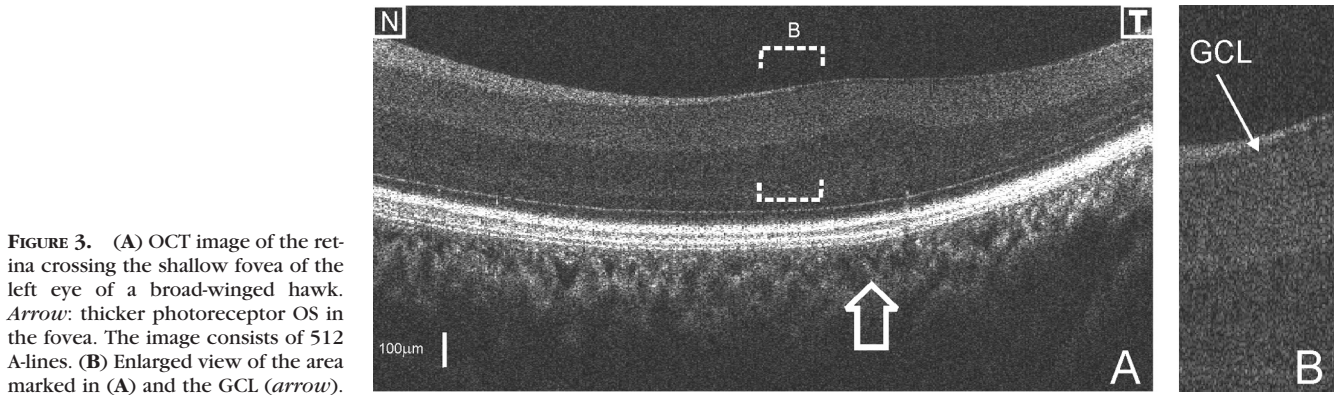


FIGURE 3. (A) OCT image of the retina crossing the shallow fovea of the left eye of a broad-winged hawk. *Arrow*: thicker photoreceptor OS in the fovea. The image consists of 512 A-lines. (B) Enlarged view of the area marked in (A) and the GCL (*arrow*).

in the OCT image from the top to the bottom. The RNFL is distinguishable as a bright band at the top of the OCT image, which shows relatively higher backscattering. The GCL was not observed as a separate layer in this dataset. Bands of relatively high and low backscattering are visible farther down into the retina that correspond to the inner plexiform layer (IP), the inner nuclear layer (IN), the outer plexiform layer (OP), and the outer nuclear layer (ON). The external limiting membrane (ELM) is visualized as a thin, bright line. Also shown in the image is the junction between the inner segment (IS) and the outer segment (OS) of the photoreceptors. The OS has much higher scattering than does the IS. Beyond the photoreceptor layers, a bright band matches the retinal pigment epithelium (RPE) complex, which separates the retina from the choroid. We clearly saw that the RPE complex consisted of a thin, low-scattering layer bordered by two distinctive bright lines. Distal to the RPE complex, a heterogeneous scattering layer is visible, where the regions of lower backscattering are attributable to the choroidal vessels (C). The absence of blood vessels in the OCT images confirms the retina's known avascularity.

The OCT image crossing the deep fovea of the hawk retina extracted from a different dataset acquired on the same eye is shown in Figure 2A. The image shows the deep fovea at its deepest point. We can see that the edges are pronounced and its depth is approximately 66% of the total retinal thickness. The relative depth of the fovea compared well with those measured with histology in raptors.¹¹ All the retinal layers in the deep foveal region seem to be the same as the ones described in Figure 1A, except that we observed a dark thin layer next to the fovea and lying underneath the RNFL that is possibly associated with the ganglion cell layer (GCL; Fig. 2A). Figure 2B shows an enlarged view of the area marked in Figure 2A, where the GCL is indicated. Whether there is a layer of extended photoreceptor axons surrounding the fovea could not be discerned in these images.

The cross-sectional image in Figure 3A shows a feature that appears to correspond to the shallow fovea of the hawk retina. In this circumstance, contrary to what has been previously described in raptors, the "shallow fovea" in this bird seems not to be a depression but a modest retinal thickening.^{1,11,14} Whether this is a characteristic of an individual bird or of the entire species is unknown. The photoreceptor outer segments appear thickened in this region, suggesting a higher photoreceptor density. Also evident in Figure 3A is a dark thin layer near the retinal thickening and lying underneath the RNFL. We believe that this thin, dark layer is associated with the GCL as we proposed for the deep fovea. Figure 3B shows an enlarged view of the area marked in Figure 3A that better shows the GCL.

Figure 4A shows an OCT image extracted from a different dataset acquired on the same hawk eye and crossing the base

of the pecten at the ONH. The OCT image shows that the pecten protrudes into the vitreous.

The OCT images in several different datasets had to be registered, to find the spatial relationship among the two foveae and the ONH. In human and rodent retinal imaging, we usually use retinal blood vessel patterns on the reconstructed OCT fundus image as landmarks to register OCT images in different scan areas. Since there are no blood vessel landmarks in the bird's retina, it was not possible to register the OCT images by this method. However, we were able to register the images by using the distribution of the RNFL's thickness. RNFL thickness generally decreases with distance from the ONH, reaches a minimum in the foveal regions,¹ and provided a means to correlate the location of the nasal and temporal foveal areas with the ONH position. RNFL thickness maps of four OCT datasets of the left eye of the hawk were calculated by manually segmenting the RNFL borders in the OCT images. The calculated RNFL thickness maps were registered according to the thickness distribution of each map. Figure 5 shows the result of the composite RNFL thickness map. Figures 5a and 5b are the thickness maps calculated from the datasets covering the deep fovea and the base of the pecten at the ONH, respectively. Figures 5c and 5d are the thickness maps derived from the two datasets covering the base of the pecten and the shallow fovea, respectively. The locations of the foveae were marked on the composite RNFL thickness map according to the cross-sectional images (Figs. 5a, 5d, white circles). The deep fovea is located on the left side of the optic nerve (nasal region), and the shallow fovea is on the right side (temporal region), as expected for the left eye of the hawk.^{1,13} The locations of the OCT images in Figures 2A, 3A, and 4 are shown as horizontal white lines in Figure 5. The diagram of the red-tailed hawk (*Buteo borealis*) fundus reported in Wood¹⁴ is shown in Figure 5e for orientation of the bird fundus.

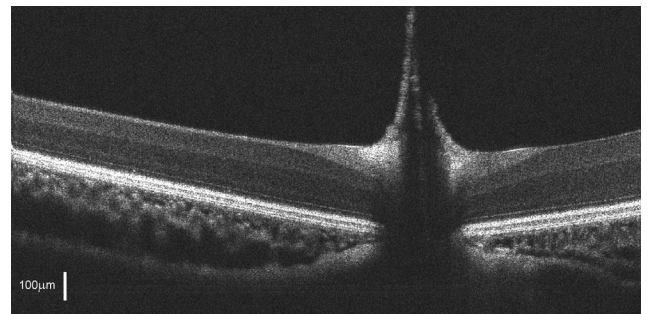


FIGURE 4. OCT image crossing the pecten at the ONH of the left eye of a broad-winged hawk. The image consists of 2048 A-lines. The pecten protrudes into the vitreous, as expected.

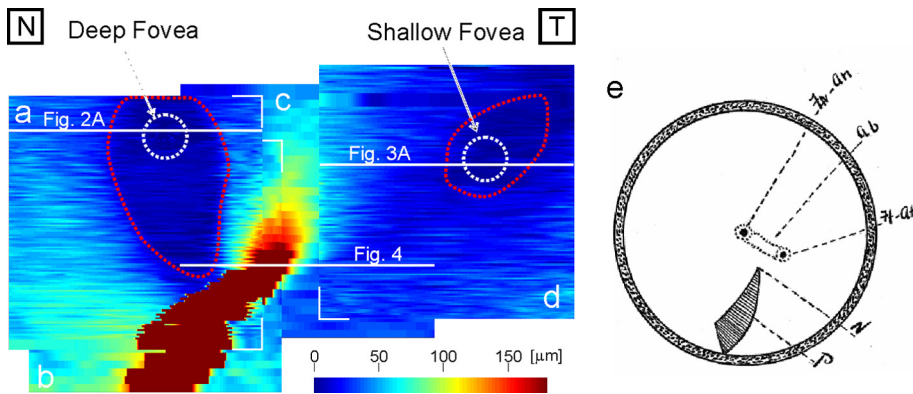


FIGURE 5. (a–d) Composite RNFL thickness map of the broad-winged hawk retina. *Red dashed lines:* the approximate margins of areas with a thicker GCL. The datasets corresponding to the thickness maps in (a) and (d) consist of 512×128 A-lines, whereas the datasets corresponding to the thickness maps in (b) and (c) consist of 2048×32 A-lines. *Horizontal white lines:* the locations of the OCT images in Figures 2A, 3A, and 4. (e) Diagram of the fundus of the red-tailed hawk (*Buteo borealis*).¹⁴ N, optic nerve entrance; P, pecten; Ft, temporal fovea (shallow fovea); Fn, nasal fovea (deep fovea).

For each cross-sectional image in the Figure 5a and 5d datasets, we determined the approximate edge of the thick perifoveal GCL. This determination was easily made for the deep fovea (Fig. 5a dataset), where the transition from thick GCL to thicker RNFL was abrupt (Fig. 2A), and possible, but less accurate, for the shallow fovea (Fig. 5d dataset), where the transition was more gradual (Fig. 3A). The boundaries of the two oblong areas of thick GCL are shown as dotted red lines in Figure 5. The area surrounding the deep fovea was large and extended nearly to the ONH, whereas that surrounding the shallow fovea was smaller, with a tail that extended away from the ONH.

We imaged a bird of another hawk species, the short-tailed hawk. The OCT images of the deep and shallow foveae are shown in Figures 6A and 6C, respectively. Compared with the images of the broad-winged hawk in Figures 2 and 3, the differences in the topography of the foveae between the two hawk species are significant. In the vicinity of the deep fovea of the short-tailed hawk, the retina is elevated into the vitreous before going down to the foveal pit, whereas in the broad-winged hawk the retina in the corresponding area is flat. The most significant difference is the topography of the shallow fovea: a dip in Figure 6 versus a hump in Figure 3. The depth

of the shallow fovea in Figure 6C is approximately 34% of the total retinal thickness, which is in good agreement with raptor histology reported in another study.¹¹ All the anatomic layers of the short-tailed hawk retina can be clearly recognized in the OCT image (Fig. 6B).

The OCT images revealed significant variations of the topography of the retina among different species of raptor. Unlike the images of human retina, the OCT images of raptors also showed the choroid clearly. Figure 7 shows two cross-sectional OCT images of the retina of a barred owl. We can see clearly the choroidal structure. From all the images we can see that the choroidal thickness changes with location: thinnest at the ONH while thickest around the foveae.

The OCT images also revealed differences in the photoreceptor layers among the different species of raptors as shown in Figure 8. In the figure, magnified OCT images of the short-tailed hawk (Fig. 8A), broad-winged hawk (Fig. 8B), great horned owl (Fig. 8C), and barred owl (Fig. 8D) are put side by side for comparison. The images were taken in the area of the foveae in the hawk and the area close to the ONH in the owl. One common feature for all the raptors is that the photoreceptor OS is thicker than the IS, whereas the feature is more significant in the great horned owl. Another common feature is

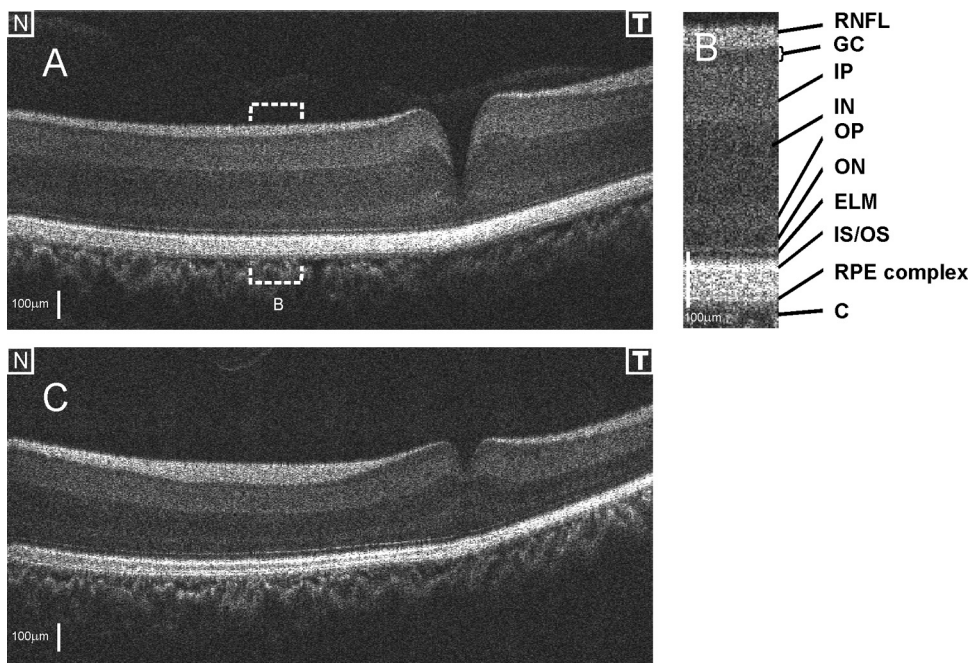


FIGURE 6. OCT images of a short-tailed hawk retina in the right eye. (A) The deep fovea; (B) twofold magnification of area marked in (A). The retinal anatomic structures were labeled as in Figure 1, including the GCL (GC). (C) shallow fovea. The OCT images consist of 512 A-lines.

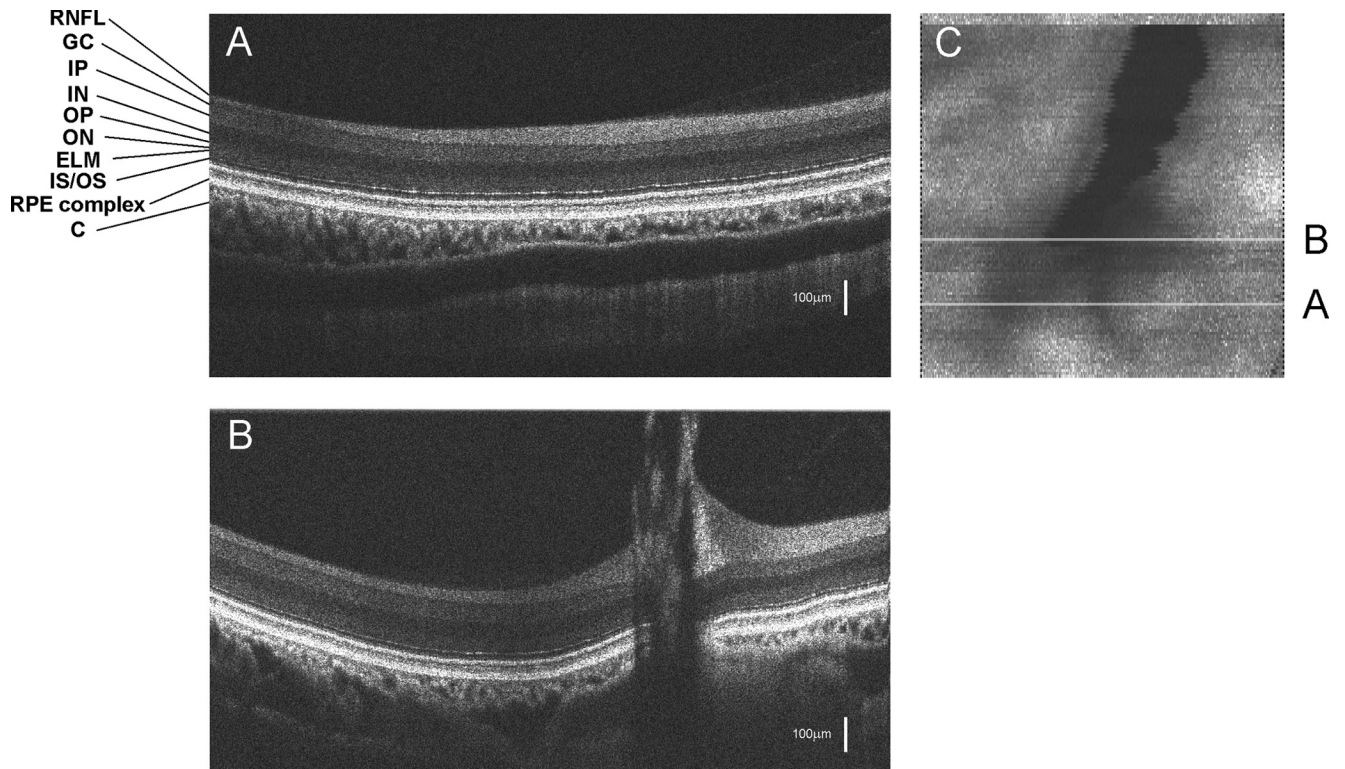


FIGURE 7. (A) OCT image of a barred owl retina. (B) OCT image of the retina crossing the pecten. (C) OCT fundus images that show the relative locations of images (A) and (B). The OCT images in (A) and (B) consist of 512 A-lines.

that the OS is high-scattering whereas the inner segment is low-scattering. However, the scattering of the OS of the hawk is generally higher than that of the owl. The barred owl has multiple layers in its OS. We hypothesize that the difference in scattering in the photoreceptor OS is related to the density of cones and rods. Since the birds cannot be killed, no histology can be obtained for the present study. The right eye of the

broad-winged hawk was known to be blind, from an unknown injury, and so it was also imaged to demonstrate the capabilities of the technology. Figure 9 shows two cross-sectional images of the retina of the right eye together with the OCT fundus image. The retinal lesions with strong evidence of traumatic injury can be clearly seen in these images. In Figure 9A, there appears to be a complete chronic retinal detachment

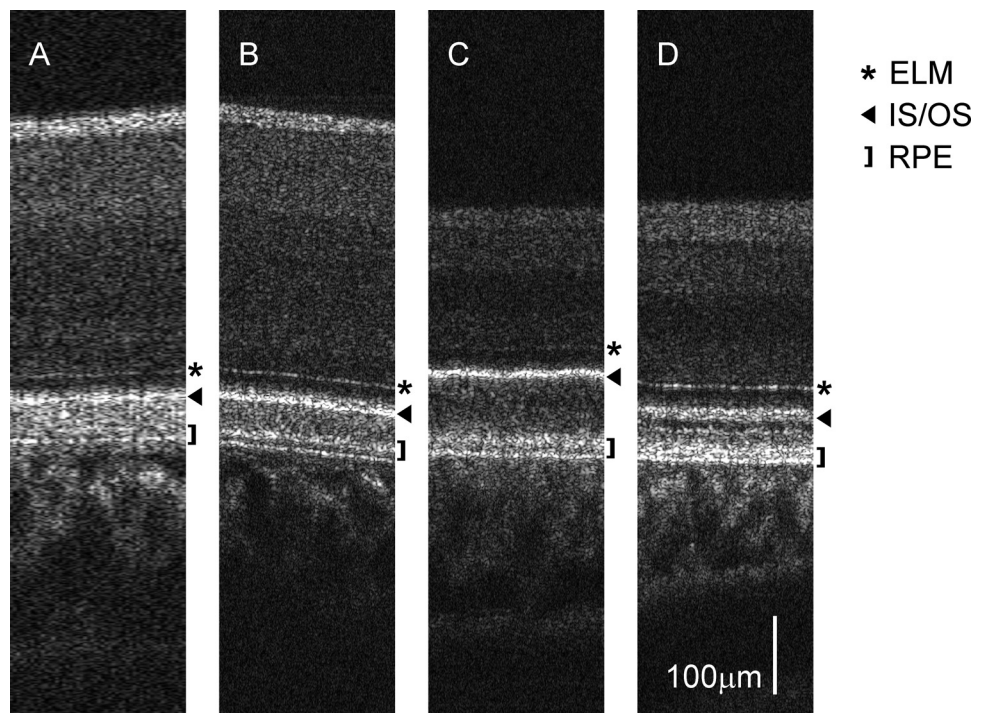


FIGURE 8. Comparison of the enlarged OCT images of the retina among the short-tailed hawk (A), broad-winged hawk (B), great horned owl (C), and barred owl (D). Images (A) and (B) are close to the deep fovea. Images (C) and (D) are close to the base of the pecten. Image (A) consists of 40 A-lines, and images (B-D) consist of 160 A-lines.

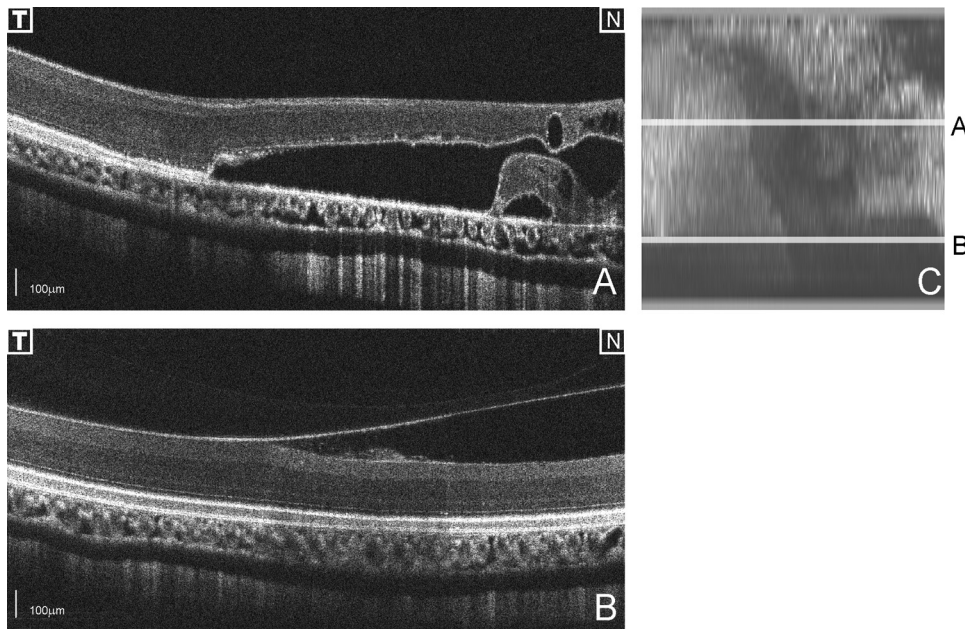


FIGURE 9. (A, B) OCT images of the retina of a broad-winged hawk's right eye that show traumatic retinal injury. (C) OCT fundus image in which the spatial location of the images (A) and (B) are marked.

(RD), with the presence of subretinal as well as proteinaceous fluid. Intraretinal cystic spaces are also visible, especially where the retina appears atrophic and thinned. There appears to be a posterior hyaloid detachment. The RPE underlying the RD appears atrophic as well. The RPE and choriocapillaris appear attenuated beneath the chronic RD.

CONCLUSION

For the first time, the retinas of raptors were imaged *in vivo* with ultra-high resolution SD-OCT. The technology provided 3-D images with $2.8 \mu\text{m}$ axial resolution. The cross-sectional images clearly demonstrated all retinal layers. The acquired datasets covered areas that subtended $32^\circ \times 32^\circ$ of visual angle. Images of unique features such as the deep and shallow foveae and the pecten could then be located in these datasets.

Datasets could be combined to provide composite images over large retinal areas. One such map (Fig. 5) demonstrated that the RNFL avoided the two foveae of the broad-winged hawk as it coursed toward the ONH. The shallow fovea of the broad-winged hawk was shown not to be a depression, but a thickened area of higher photoreceptor and ganglion cell density (Fig. 3), a finding that should be confirmed in more members of this species. Both foveae of the short-tailed hawk, on the other hand, showed the expected morphology. The OCT images also confirmed the anangiotic feature of the raptor retina.

Traumatic injuries to a bird's retina were imaged with high quality. Although the images shown were obtained with an ultra-high resolution research instrument, commercially available SD-OCT instruments that now achieve $\sim 6 \mu\text{m}$ axial resolution should be capable of demonstrating many of the reported observations. The results show that high-resolution OCT is a powerful imaging tool for vision research in birds of prey, which may also have clinical applications.

Acknowledgments

The authors thank William Hodos, PhD (University of Maryland Department of Psychology), for scientific consultations and comments on the manuscript; Hassan Wehbe, a former student at the Optical Coherence Imaging Research Laboratory (Bascom Palmer Eye Institute) for

help in collecting several sets of OCT data; and Greta Parks-Mealey, Director of Wildlife Center and Falcon Batchelor Bird of Prey Center, Miami Science Museum for giving access to the birds and help in handling them.

References

1. Walls GL. *The Vertebrate Eye and Its Adaptive Radiation*. Bloomfield Hills: Crankbook Institute of Science; 1963.
2. Jones MP, Pierce KE Jr, Ward D. Avian vision: a review of form and function with special consideration to birds of prey. *J Exotic Pet Med*. 2007;16(2):69–87.
3. Fite KV. Anatomical and behavioral correlates of visual acuity in the great horned owl. *Vision Res*. 1973;13:219–230.
4. Butler AB, Hodos W. *Comparative Vertebrate Neuroanatomy: Evolution and Adaptation*. New York; Wiley-Liss; 1996.
5. Curcio CA, Allen KA. Topography of ganglion cells in human retina. *J Comp Neurol*. 1990;300:5–25.
6. Gunturkun O. Sensory physiology: vision. In: Whittow GC, ed. *Sturkie's Avian Physiology*. 5th ed. Academic Press, San Diego; 2000.
7. Hughes A. The topography of vision in mammals of contrasting lifestyle: comparative optics and retinal organization. In: Crescitelli FM, ed. *The Visual System in Vertebrates*. New York: Springer-Verlag; 1977;613–756.
8. Kiama SG, Maina JN, Bhattacharjee J, Weyrauch KD. Functional morphology of the pecten oculi in the nocturnal spotted eagle owl (*Bubo bubo africanus*), and the diurnal black kite (*Milvus migrans*) and the domestic fowl (*Gallus gallus domesticus*): a comparative study. *J Zool (Lond)*. 2001;254:521–528.
9. Samuelson D. Ophthalmic anatomy. In: Gelatt KN, ed. *Veterinary Ophthalmology*. 3rd ed. Baltimore, MD, Lippincott Williams & Wilkins, 1991;31–150.
10. Meyer DB. The avian eye and its adaptations. In: Crescitelli F, ed. *The Visual System in Vertebrates*. New York: Springer-Verlag; 1977:611–649.
11. Fite KV, Rosenfield-Wessels S. A comparative study of deep avian foveas. *Brain Behav Evolut*. 1975;12:97–115.
12. Murphy CJ. Raptor ophthalmology. *Compend Cont Educ Pract Vet*. 1987;9(3):241–260.
13. Tucker VA. The deep fovea, sideways vision and spiral flight paths in raptors. *J Exp Biol*. 2000;203:3745–3754.
14. Wood CA. *The Fundus Oculi of Birds Especially as Viewed by the Ophthalmoscope*. Chicago: Lakeside Press; 1917.

15. Gumpenberger M, Kolm G. Ultrasonographic and computed tomographic examinations of the avian eye: physiologic appearance, pathologic findings, and comparative biometric measurement, *Vet Radiol Ultrasound*. 2006;47:492-502.
16. Srinivasan VJ, Ko TH, Wojtkowski M, et al. Noninvasive volumetric imaging and morphometry of the rodent retina with high-speed, ultrahigh-resolution optical coherence tomography. *Invest Ophthalmol Vis Sci*. 2006;47:5522-5528.
17. Ruggeri M, Tschepnakis G, Jiao S, et al. Retinal tumor imaging and volume quantification in mouse model using spectral domain optical coherence tomography. *Opt Express*. 2009;17:4074 - 4083.
18. Ruggeri M, Wehbe H, Jiao S, et al. In vivo three-dimensional high-resolution imaging of rodent retina with spectral-domain optical coherence tomography. *Invest Ophthalmol Vis Sci*. 2007;48:1808-1814.
19. Huang Y, Cideciyan AV, Papastergiou GI, et al. Relation of optical coherence tomography to microanatomy in normal and rd chickens. *Invest Ophthalmol Vis Sci*. 1998;39:2405-2416.
20. Jiao S, Knighton R, Huang X, Gregori G, Puliafito CA. Simultaneous acquisition of sectional and fundus ophthalmic images with spectral-domain optical coherence tomography. *Opt Express*. 2005;13:444 - 452.